Cellular Physiology and Biochemistry

Cell Physiol Biochem 2018;50:1414-1428
DOI: 10.1159/000494604
Published online: 25 October 2018
Accepted: 17 October 2018

Original Paper

Blood-Stage Plasmodium Berghei ANKA Infection Promotes Hepatic Fibrosis by Enhancing Hedgehog Signaling in Mice

Jieun Kim[a] Sihyung Wang[a] Chanbin Lee[a] Sumi Sung[a] Yongbo Shin[a] Kyoung Seob Song[c] Hee-Jae Cha[d] Meesun Ock[d] Youngmi Jung[a,b]

[a]Department of Integrated Biological Science, College of Natural Science, Pusan National University, Pusan, [b]Department of Biological Sciences, College of Natural Science, Pusan National University, Pusan, [c]Department of Physiology, Kosin University College of Medicine, Pusan, [d]Department of Parasitology and Genetics, Kosin University College of Medicine, Pusan, South Korea

Key Words
Plasmodium berghei ANKA • Liver • Fibrosis • Hedgehog

Abstract
Background/Aims: Malaria is the most deadly parasitic infection in the world, resulting in damage to various organs, including the liver, of the infected organism; however, the mechanism causing this damage in the liver remains unclear. Liver fibrosis, a major characteristic of liver diseases, occurs in response to liver injury and is regulated by a complex network of signaling pathways. Hedgehog (Hh) signaling orchestrates a number of hepatic responses including hepatic fibrogenesis. Therefore, we investigated whether Hh signaling influenced the liver's response to malarial infection. ***Methods:*** Eight-week-old male C57BL/6 mice inoculated with blood containing *Plasmodium berghei* ANKA (*Pb*A)-infected erythrocytes were sacrificed when the level of parasitemia in the blood reached 10% or 30%, and the livers were collected for biochemical analysis. Liver responses to *Pb*A infection were examined by hematoxylin and eosin staining, real-time polymerase chain reaction, immunohistochemistry and western blot. ***Results:*** Severe hepatic injury, such as ballooned hepatocytes, sinusoidal dilatation, and infiltrated leukocytes, was evident in the livers of the malaria-infected mice. Hypoxia was also induced in 30% parasitemia group. With the accumulation of Kupffer cells, inflammation markers, TNF-α, interleukin-1β, and chemokine (C-X-C motif) ligand 1, were significantly upregulated in the infected group compared with the control group. Expression of fibrotic markers, including transforming growth factor-β, α-smooth muscle actin (α-SMA), collagen 1a1, thymosin β4, and vimentin, were significantly higher in the infected groups than in the control group. With increased collagen deposition, hepatic stellate cells expressing α-SMA accumulated in the liver of the *Pb*A-infected mice, whereas those cells were rarely detected in the livers of the control mice. The levels of Hh signaling and Yes-associated protein (YAP), two key regulators for hepatic fibrogenesis, were significantly elevated in the infected groups

Dr. Youngmi Jung
Department of Biological Sciences, College of Natural Science, Pusan National University
63-2 Pusandaehak-ro, Geumjeong-gu, Pusan 46241 (Republic of Korea)
Tel. +82-51-510-2262, Fax +82-51-581-2962, E-Mail y.jung@pusan.ac.kr

compared with the control group. Treatment of mice with Hh inhibitor, GDC-0449, reduced hepatic inflammation and fibrogenesis with Hh suppression in *Pb*A-infected mice. ***Conclusion:*** Our results demonstrate that HSCs are activated in and Hh and YAP signaling are associated with this process, contributing to increased hepatic fibrosis in malaria-infected livers.

Introduction

Malaria is one of the most life-threatening infectious diseases in the world and remains a major global health burden in many tropical countries [1]. Most malarial deaths are due to infection with *Plasmodium falciparum (P. falciparum)*, which is a protozoan parasite that causes severe malaria and complications in humans. The protozoa induce stage-specific pathological changes, including asymptomatic changes during the liver stage and symptomatic changes during the erythrocyte stage [2, 3]. In the erythrocyte stage, red blood cells parasitized by protozoa become sequestered in small blood vessels and induce local blood flow impairment, leading to disturbances and failure in various organs, including the liver [4]. Several studies have reported oxidative stress, hypoxia, increased inflammation, and hepatocyte apoptosis in malaria-infected livers [5, 6]. Liver dysfunction, such as jaundice, hepatomegaly, and liver enzyme elevation, have been reported in patients with *P. falciparum* [7-9], but malarial hepatopathy remains poorly understood. Patients with malaria infection die with organ failure including liver [10, 11]. However, most of researches focus on other organs, not liver. Although a few clinical and experimental studies reported malaria-induced liver damage, most studies have showed liver stage development of malaria parasites for vaccine development rather than treatment [2, 3]. Hence, its underlying mechanism remains poorly understood.

Liver fibrosis that is characterized by an excessive accumulation of extracellular matrix (ECM) proteins is the major determinant of morbidity and mortality in patients with liver disease [12]. Following liver injury of any cause, hepatic stellate cells (HSCs) become activated and transdifferentiate from quiescent (Q-) HSCs into myofibroblastic (MF-) HSCs, which are the main collagen-producing cells. Oxidative stress, hypoxia, and inflammation are known to stimulate HSC activation [12]. The Hh signaling pathway is one of cytokines regulating HSC activation [13-15]. Smoothened (Smo), an Hh receptor, is released into the cytoplasm through the binding of Hh ligands, Sonic Hh (Shh), Indian Hh (Ihh) and Desert Hh (Dhh), to Patched (Ptc), and activates Glis by blocking Glis degradation [16]. The activated Glis act as transcriptional factors and turn on their own signaling pathway and pro-fibrotic response-related genes. Hh signaling, which is rarely detected in healthy adult livers, is activated in response to liver damage and orchestrates tissue remodeling [16, 17]. Apoptotic hepatocytes in the injured liver secrete Hh ligands, Ihh, and Shh, which trigger HSC activation by turning on the Hh signaling pathway in HSCs [15, 18, 19]. These Hh-responsive HSCs accelerate HSC transition into MF-HSCs in a paracrine or autocrine manner, contributing to liver fibrosis. Hh ligands are also involved in the recruitment of inflammatory cells and promote liver inflammation [16, 17]. However, it remains unclear whether and how the fibrotic response occurs in malaria-infected livers. Given the increased inflammation and apoptotic hepatocytes in malaria-infected livers [5, 20], we hypothesize that liver fibrosis increases and Hh signaling is involved in the response to malaria infection. Herein, we employ an experimental murine model of erythrocytic malaria infection using *Plasmodium berghei* ANKA (*Pb*A), one of the experimental models of malaria [21-23], and demonstrate that Hh signaling is activated and promotes hepatic fibrosis and inflammation in livers damaged by *Pb*A infection, suggesting the potential role of Hh in hepatopathy following malaria infection.

Materials and Methods

Mice and experimental infections

Male C57BL/6 mice at 7 weeks old were purchased from Hyochang (Dae-gu, Korea), fed with normal diet, watered, and housed with a 12 h light-dark cycle. Mice were infected via tail vein injection with 10^6 *Pb*A-infected red blood cells (iRBCs) [24, 25]. As a control, mice were injected with the same volume of PBS (n=4). Following infection, survival and mortality was monitored daily. After infection of *Pb*A-iRBCs, C57BL/6 mice were sacrificed when parasitemia reached 10 or 30 % (n=5 per group), and the liver tissue was collected for histological and biochemical analysis. Parasitemia was assessed by determining the percentage of parasitized RBCs in Giemsa-stained thin smears using blood from the tail vein under a microscope. RBC counts were performed with a hematocytometer, and more than 1000 RBCs were counted by light microscopy (x100) to determine the percentage of parasitized cells. Animal care and surgical procedures were approved by the Kosin University College of Medicine Institutional Animal Care and Use Committee (KMAP-15-09) and carried out in accordance with the provisions of the NIH Guide for the Care and Use of Laboratory Animals.

Treatment of Hh Inhibitor, GDC-0449

To investigate the effect of Hh inhibitor on blood stage infection in liver, mice were treated with dimethyl sulfoxide (DMSO) or Smo antagonist GDC-0449 (Vismodegib; Selleck Chemicals, Houston, TX). Following *Pb*A-infection (n=10), mice were randomly divided into two groups (n=5 per group); 25mg/kg of GDC-0449 or DMSO was injected into mice by intraperitoneal injection. As the control groups, mice without *Pb*A infection were injected with equal volume or concentration of vehicle or GDC-0449 (n=4 per group). The dose of GDC-0449 was decided based on the previous our study [26]. All mice were sacrificed when the parasitemia of DMSO-treated *Pb*A-infected mice reached 10% to collect tissue and serum.

Liver histology and Immunohistochemistry

Liver specimens were fixed in 10% neutral buffered formalin, dehydrated, embedded in paraffin and cut into 4 μm section. Specimens were dewaxed, hydrated, and stained usual method with standard hematoxylin and eosin staining (H&E) for evaluation of pathologic changes. For immunohistochemical staining, sections were incubated for 10 min in 3% hydrogen peroxide to block endogenous peroxidase. Antigen retrieval was performed by heating in 10 mM sodium citrate buffer (pH 6.0) for 10 min or incubation with pepsin for 10 min. Sections were treated with Dako protein block (X0909; Dako, Carpinteria, CA, USA) for 30 min and incubated with primary antibody against αSMA (ab5694; Abcam, Cambridge, MA, USA) or F4/80 (ab6640; Abcam) at 4°C overnight. Polymer horseradish peroxidase (HRP) anti-rabbit (K4003; Dako) and anti-rat IgG-HRP (sc-2006; Santa Cruz Biotechnology, Inc., CA, USA) was used as secondary antibody. 3, 3'-Diaminobenzidine (DAB) was employed in the detection procedure. The sections were counterstained with hematoxylin and positive cells were identified by dark-brown staining. For double immunofluorescent staining, liver sections were incubated with primary antibody, rabbit anti-YAP (4912; Cell Signaling Technology, Inc.) and mouse anti-αSMA (A5228; Sigma-Aldrich, St Louis, MO, USA) for 4°C overnight. The fluorescein labelled anti-rabbit IgG (Alexa Fluor 568, Invitrogen, Carlsbad, CA) and anti-mouse IgG (Alexa Fluor 488, Invitrogen) were used as secondary antibodies for 30 min. 4',6-diamidino-2-phenylinole (DAPI) were employed in the counterstaining procedure.

Histological assessments and Cell counting

For histological assessments, 10 central vein (CV) areas were randomly selected per section at ×20 magnifications for each mouse. Based on criteria described in previous studies [27], sinusoidal dilatation was scored as follows: Grade 0, normal; Grade 1, visible sinusoidal space; Grade 2, early dilatation around CV; Grade 3, a generalized dilatation around CV looking like medusa head. The unit of sinusoidal dilatation score is the sum of grades measured in

10 fields of each mice. Inflammatory foci were considered as the accumulation of inflammatory cells in number higher than 10 cells per field for each mouse. To quantify the number of F4/80-positive cells, 10 areas were randomly selected per section at × 40 magnification for each mouse. The F4/80-positive cells were quantified by counting the total number of F4/80-positive cell per field and dividing by the total number of hepatocytes per field.

Table 1. Sequences of primers used for QRT-PCR. Primer sequences shown in this table were used for real-time qRT-PCR. All values were normalized to the level of 9S for total mRNA

Gene	Forward Sequence	Reverse Sequence
9s	GACTCCGGAACAAACGTGAGG	CTTCATCTTGCCCTCGTCCA
Tnfa	TCGTAGCAAACCACCAAGTG	AGATAGCAAATCGGCTGACG
Il1b	ACTCCTTAGTCCTCGGCCA	TGGTTTCTTGTGACCCTGAGC
Cxcl1	CCCAAACCGAAGTCATAGCC	TCAGAAGCCAGCGTTCACC
Tgfb1	TTGCCCTCTACAACCAACACAA	GGCTTGCGACCCACGTAGTA
aSma	AAACAGGAATACGACGAAG	CAGGAATGATTTCCAAAGGA
Col1a1	GAGCGGAGAGTACTGGATCG	GCTTCTTTTCCTTGGGGTTC
Tb4	ATGTCTGACAAACCCGATATGGC	CCAGCTTGCTTCTCTTGTTCA
Vimentin	GCTTCTCTGGCACGTCTTGA	CGCAGGGCATCGTTGTTC
Bmp7	GTGGTCAACCCTCGGCACA	GGCGTCTTGGAGCGATTCTG
Ecadherin	ACCTCTGGGCTGGACCGA	CCTGATACGTGCTTGGGTTGAA

Quantitative real-time PCR

Total RNA was extracted from liver tissues or cells with TRIzol reagent (Ambion, Thermo Fisher Scientific, Waltham, MA, USA). The concentration and purity of RNA were determined using a nanodrop. Template cDNA was synthesized from total RNA using the SuperScript First-strand Synthesis System (Invitrogen, Thermo Fisher Scientific) according to the manufacturer's protocols. We performed the real-time quantitative reverse transcriptional polymerase chain reaction (qRT-PCR) analysis by using the Power SYBR Green Master Mix (Applied Biosystems, Thermo Fisher Scientific) according to the manufacturer's specifications (Eppendorf, Mastercycler Real-Time PCR). All reactions were triplicated and the data were analyzed according to the $\Delta\Delta C_t$ method. The 40S ribosomal protein 9S mRNA for mRNA was used to normalize expression levels. The sequences of all primers used in this study are summarized in Table 1. All PCR products were directly sequenced for genetic confirmation (Macrogen, Seoul, Korea).

Western blot assay

Total protein was extracted from freeze-clamped liver tissue sample that had been stored at -80°C. Whole tissues were homogenized in Triton-lysis buffer (TLB) supplemented with protease inhibitors (Roche, Indianapolis, IN, USA). The supernatants containing whole protein extract were used in subsequent biochemical analysis. For Gli2 or YAP detection, nuclear/cytosolic fractionation was performed as described previously [28]. Briefly, cells were homogenized and suspended in buffer A (10 mM HEPES, 50 mM NaCl, 1 mM DTT, 0.1 mM EDTA, 0.1 mM PMSF) with protease inhibitors (Roche) and incubated on ice for 20 min. An equal volume of buffer B (buffer A + 0.1% NP-40) was added and the lysates were incubated for 20 min on ice. After centrifugation at 5000 × g for 2 min, the supernatant was collected for the cytosolic fraction. The pellets were resuspended with buffer C (10 mM HEPES, 400 mM NaCl, 1 mM DTT, 1 mM EDTA, 1 mM PMSF, 1 mM EGTA) and incubated on ice for 30 min. After centrifugation at 13000 rpm for 15 min, the supernatant was saved for the nuclear fraction. Equal amounts of protein were fractionated by polyacrylamide gel electrophoresis and transferred to PVDF (polyvinylidene difluoride) membranes. Primary antibodies against HIF1a (NB100-105; Novus Biologicals, Littleton, CO, USA), αSMA (A5228; Sigma-Aldrich, St Louis, MO, USA), TGFβ (3711S; Cell Signaling Technology, Inc., Danvers, MA, USA), SHH (sc-9024; Santa Cruz Biotechnology, Inc.), SMO (ab7213; Abcam), GLI2 (GWB-CE7858; GenWay Biotech, Inc., San Diego, CA, USA), YAP (4912; Cell Signaling Technology, Inc.), phosphor-YAP (4911; Cell Signaling Technology, Inc.) and GAPDH (MCA4739; AbD Serotec, Oxford, UK) were used in this experiment. Horseradish peroxidase (HRP)-conjugated anti-rabbit or anti-mouse IgG (Amersham ECL™, GE Healthcare, Milwaukee, WI, USA) was used as the secondary antibody. Protein bands were detected using an EzWestLumi ECL solution

(ATTO Corporation, Tokyo, Japan) per the manufacturer's specifications (ATTO Corporation, Ez-Capture II). Protein-band density was measured using CS Analyzer software (Version 3.00.1011, ATTO & Rise Corporation).

Hydroxyproline assay

The hydroxyproline content of the livers was calculated by the method previously described [28]. Briefly, 50 mg of freeze-dried liver tissue was hydrolyzed in 6 N HCL at 110°C for 16 h. The hydrolysate was evaporated under vacuum and the sediment was re-dissolved in 1 ml of distilled water. Samples were filtered in a 0.22 μm filter centrifuge tube at 14, 000 rpm for 5 min. Lysates were then incubated with 0.5 ml of chloramine-T solution containing 1.41 g of chloramine-T dissolved in 80 ml of acetate–citrate buffer and 20 ml of 50% isopropanol at RT. After 20 min, 0.5 ml of Ehrlich's solution containing 7.5 g of dimethylaminobenzaldehyde dissolved in 13 ml of 60% perchloric acid and 30 ml of isopropanol were added to the mixture, which was incubated at 65°C for 15 min. After cooling to RT, the absorbance was read at 561 nm. The amount of hydroxyproline in each sample was determined using the regression curve from the sample prepared with high-purity hydroxyproline (Sigma-Aldrich) and divided by the liver weight of the initial sample (50 mg) to calculate hydroxyproline content (μg hydroxyproline per mg liver). Data were expressed as fold changes by comparing with hydroxyproline content of the control group.

Measurement of ALT and AST

Serum alanine transaminase (ALT/GPT, glutamate-pyruvate transaminase) and aspartate transaminase (AST/GOT, glutamate-oxaloacetate transaminase) levels were measured using GOT and GPT reagents (Asan Pharmaceutical, Seoul, Korea) according to the manufacturer's instructions.

Statistical analysis

Results of experimental studies are expressed as mean±standard deviation (mean±SD). Statistical differences were determined by the unpaired two-sample Student's t-test. Differences were considered as significant when P-values <0.05.

Results

Malaria infection induces liver damage

To generate an experimental malaria mouse model, eight-week-old mice were injected intraperitoneally with 10^6 *Pb*A-infected red blood cells (iRBCs). Because all mice died at a 70% *Pb*A infection rate in the blood, mice with 10% and 30% infection rates were sacrificed; mice developed 10% parasitemia at 5 days and 30% parasitemia at 7 days post-infection, respectively. Liver sections from *Pb*A-infected mice were examined for morphology using H&E staining. Compared to PBS-injected mice (CON group), livers of *Pb*A-infected groups showed sinusoidal dilatation, immune infiltration, immune foci, hemozoin deposition, and portal tract inflammation (Fig. 1A). These histomorphological changes including hemozoin deposition (indicated by blue arrowheads) and apoptotic hepatocytes having Mallory bodies (indicated by yellow arrows) in the portal tract were more severe in the 30% parasitemia group than in the 10% parasitemia group. The score of sinusoidal dilatation around CV and the number of immune foci significantly increased in the infected groups compared with the CON group, and they were much higher in the 30% parasitemia group than in the 10% parasitemia group (Fig. 1B). Immunohistochemistry for F4/80, a marker of liver macrophages (kupffer cells), also showed that macrophage expressing F4/80 accumulated in the livers of *Pb*A-infected mice compared to the CON group (Fig. 1C and 1D). Since a strong inflammatory response was evident in the liver of *Pb*A-infected mice, the level of pro-inflammatory marker in the liver of these mice was assessed using qRT-PCR analysis. Expression of tumor necrosis factor-alpha (*Tnfa*), interleukin 1 beta (*Il1b*), and chemokine (C-X-C motif) ligand 1 (*Cxcl1*)

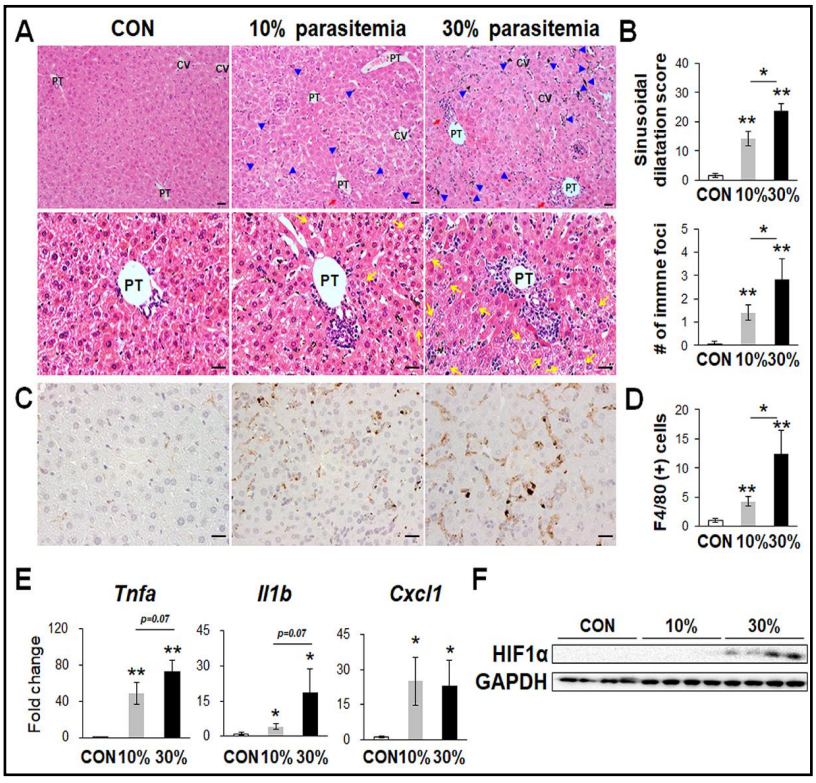

Fig. 1. Severe hepatic injury with inflammation in malaria-infected liver. (A) Representative images of H&E-stained liver sections from each group. Red and yellow arrows indicate the portal tract inflammation and apoptotic hepatocytes having Mallory bodies, respectively. Blue arrowheads indicate the hemozoin deposition and white line circles indicate the immune foci (scale bar = 20 μm). (B) The degree of sinusoidal dilatation was scored (top) and the number of inflammatory foci per field was counted (bottom). Mean±SD results are graphed (*p<0.05, **p<0.005 vs CON). (C) Representative images of F4/80-stained liver section from each group. Brown color indicate F4/80-positive cells (scale bar = 20 μm). (D) F4/80-positive cells were quantified by counting the total number of F4/80-positive cells per field. Mean±SD results are graphed (*p<0.05, **p<0.005 vs CON). (E) QRT-PCR analysis for Tnfa, Il1b and Cxcl1 of liver from each group (n ≥ 3 mice / group). Mean±SD results are graphed (*p<0.05, **p<0.005 vs CON). (F) Immunoblots for HIF1α in liver from each group (n=4 mice / group). GAPDH was used as an internal control. Data shown represent one of three experiments with similar results. (CV: central vein; PT: portal tract; CON: uninfected controls; 10%: infected mice with 10% parasitemia; 30%: infected mice with 30% parasitemia).

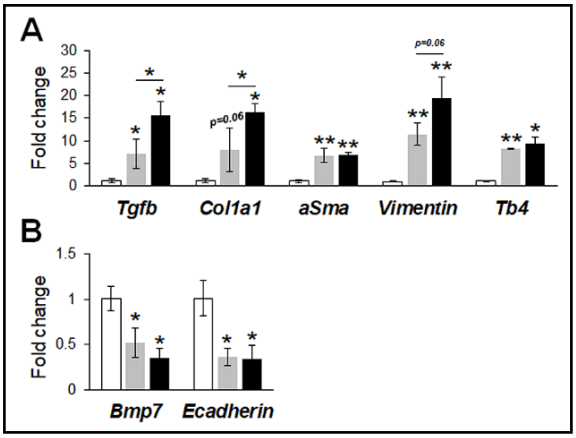

Fig. 2. Increased expression of fibrosis-related genes in the malaria-infected liver. (A) QRT-PCR analysis for Tgfb, Col1a1, aSma, Vimentin and Tb4 of liver from each group (n ≥ 3 mice / group). Mean±SD results are graphed (*p<0.05, **p<0.005 vs control). (B) QRT-PCR analysis for Bmp7 and Ecadherin (n ≥ 3 mice / group). Mean±SD results are graphed (*p<0.05, **p<0.005 vs CON). (CON: uninfected controls; 10%: infected mice with 10% parasitemia; 30%: infected mice with 30% parasitemia).

significantly increased in the infected groups compared with the CON group (Fig. 1E). The level of *Tnfa* and *Il1b* tended to be higher in the 30% parasitemia group than in the 10% parasitemia group. Because malaria infection has been known to induce tissue hypoxia in the host [29], the levels of hypoxia inducible factor-1 alpha (Hif1a) in the livers of the *Pb*A-infected mice were evaluated. HIF1α expression was rarely detected in the livers of the CON

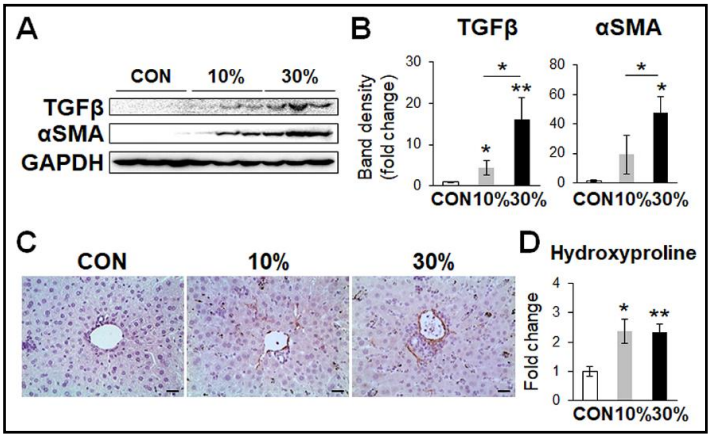

Fig. 3. Enhanced HSC activation and collagen accumulation in liver of malaria-infected mice. (A) Immunoblots for TGFβ and αSMA in liver from each group (n=3 mice / group). GAPDH was used as an internal control. Data shown represent one of three experiments with similar results. (B) Cumulative densitometric analyses of TGFβ and αSMA immunoblots are displayed as the mean±SD (*p<0.05, **p<0.005 vs CON). (C) Immunohistochemical staining for αSMA in liver sections from representative mice from each group. Brown color indicated αSMA-positive cells (scale bar = 20 μm). (D) Hepatic hydroxyproline content in liver tissues from each group (n = 3 mice / group). Mean±SD results are graphed (*p<0.05, **p<0.005 vs CON). (CON: uninfected controls; 10%: infected mice with 10% parasitemia; 30%: infected mice with 30% parasitemia).

and 10% parasitemia groups, whereas the expression of HIF1α was significantly increased in the livers of mice in the 30% parasitemia group, as assessed by western blot analysis (Fig. 1F). These results indicate that liver injury occurred in the *Pb*A-injected mice.

Hepatic fibrosis is enhanced in the livers of PbA-infected mice

Liver damage causes inflammation, which accelerates fibrosis by releasing HSC-stimulating cytokines [30-32]. Based on the severe hepatic injury with inflammation in the livers of the *Pb*A-injected mice in this study, we evaluated whether *Pb*A infection promotes liver fibrosis. The RNA levels of the pro-fibrotic promoter, Tgfb, and fibrotic markers, collagen type1 alpha1 (Col1a1), α-smooth muscle actin (aSma), vimentin, and thymosin beta 4 (Tb4), were significantly enhanced in the livers of both infected groups compared with the CON group. Among these fibrogenic markers, the expressions of *Tgfb*, *Col1a1*, and *Vimentin* showed significant increases or the tendency to increase parallel with the *Pb*A infection rate (Fig. 2A). Expressions of Q-HSC markers, bone morphogenetic protein 7 (*Bmp7*), and *Ecadherin* were downregulated in the infected groups compared with the CON group (Fig. 2B). The protein levels of TGFβ and αSMA increased in the infected groups compared with the CON group, and were greater in the 30% parasitemia group than in the 10% parasitemia group (Fig. 3A and B). Immunohistochemistry for αSMA, a marker for MF-HSCs, showed an accumulation of αSMA-positive cells in the livers of *Pb*A-infected mice whereas those cells were rarely detected in the livers of the control mice (Fig. 3C). In addition, hydroxyproline contents for the biochemical determination of deposition of collagen fibrils confirmed that the infected groups had significantly more liver fibrosis than the CON group (Fig. 3D). These results suggest that malaria infection promoted activation of MF-HSCs and hepatic fibrosis.

Hh pathway and YAP are upregulated in injured livers by malaria infection

Given that Hh signaling is known to regulate the fibrogenic response and HSC activation [13-15] and elevated fibrosis were observed in the livers of *Pb*A-infected mice, we examined whether Hh signaling was activated in these livers. The amount of SHH, an Hh ligand, SMO, an Hh receptor, and GLI2, the Hh-target gene, significantly increased in the infected groups compared with the CON group, as assessed by western blot analysis (Fig. 4A and 4B). YAP, an essential regulator of HSCs, is known to translocate into the nucleus and turns on its target genes during HSC activation [33]. Phosphorylated YAP (p-YAP) is an inactive form and degrades in the cytoplasm [34]. Although the level of total YAP and p-YAP tended to be lower in the infected groups than in the CON group, the expression of YAP in the nucleus

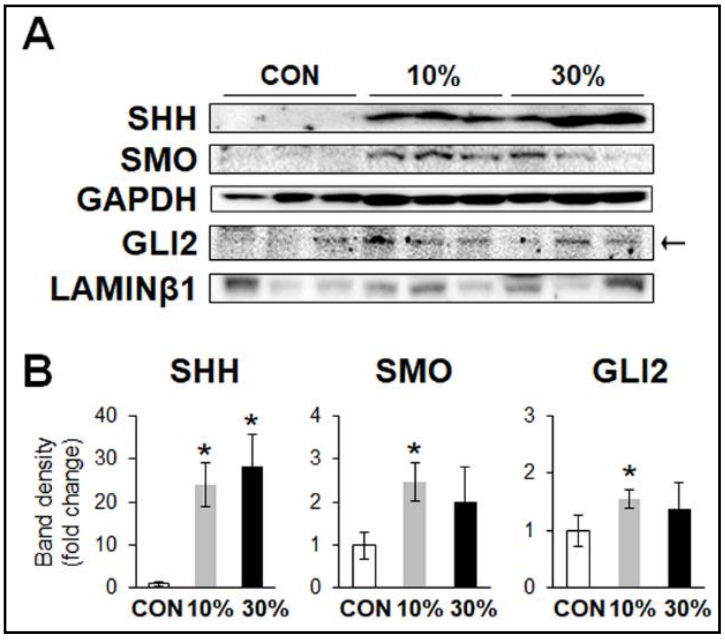

Fig. 4. Activated Hh signaling in the malaria-infected liver. (A) Immunoblots for SHH, SMO and GLI2 in liver from each group (n=3 mice / group). GAPDH or LAMINβ1 was used as an internal control. Data shown represent one of three experiments with similar results. (B) Cumulative densitometric analyses of SHH, SMO and GLI2 immunoblots are displayed as the mean±SD (*p<0.05, **p<0.005 vs CON). (CON: uninfected controls; 10%: infected mice with 10% parasitemia; 30%: infected mice with 30% parasitemia).

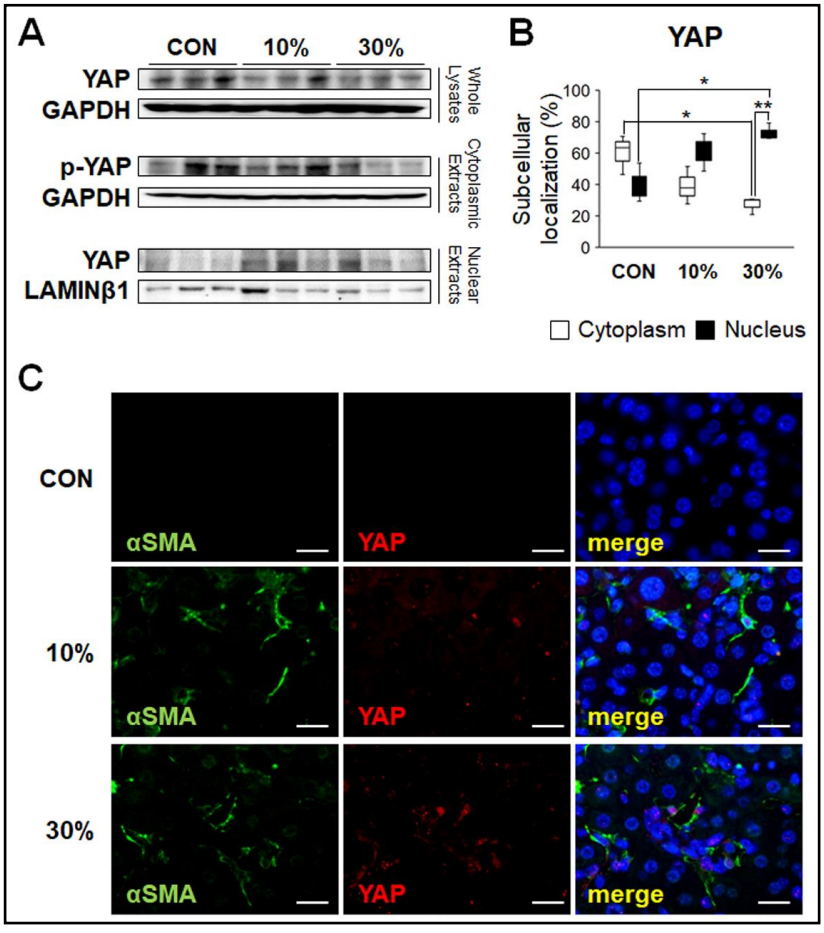

Fig. 5. Malaria infection induces activation of YAP by enhancing nuclear YAP expression. (A) Immunoblots for YAP and phosphor-YAP (p-YAP) in whole lysates, cytoplasmic extracts or nuclear extracts of liver from each group (n=3 mice / group). GAPDH or LAMINβ1 was used as an internal control. Data shown represent one of three experiments with similar results. (B) Quantification of subcellular localization of YAP in cytoplasm or nucleus from cumulative densitometric analyses of YAP and p-YAP immunoblots. Medians and ranges of results are graphed (*p<0.05, **p<0.005). (C) Double immunofluorescent staining for αSMA and YAP in liver sections from representative mice from each group. Green and red colors indicate αSMA and YAP, respectively. DAPI nuclear staining is shown as blue (scale bar = 20 μm). (CON: uninfected controls; 10%: infected mice with 10% parasitemia; 30%: infected mice with 30% parasitemia).

was evident in the infected groups compared with the CON group. Hence, we quantified the relative expression level of the active YAP, nuclear form, and the inactive YAP, p-YAP, to the total YAP by dividing the amount of active or inactive YAP by the amount of total YAP. The relative expression of p-YAP was significantly lower, but the relative expression of nuclear YAP was significantly higher in the 30% parasitemia group than in the CON group. In addition, the livers of the 30% parasitemia mice contained a greater level of active YAP than inactive YAP (Fig. 5A and B). Double immunofluorescent staining confirmed that YAP was mostly localized in the nucleus of αSMA-positive cells in the parenchymal regions of liver sections from the infected mice, whereas these double positive cells were rarely detected in the control mice (Fig. 5C). These results suggest that malaria infection leads to activation of the Hh pathway and YAP in damaged livers, implying that activation of the Hh pathway and YAP might be involved in HSC activation and fibrosis.

Suppressed Hh activity attenuates malaria-induced liver damage and hepatic fibrosis

To investigate whether the activated Hh pathway is directly associated with the liver damage after *Pb*A infection, *Pb*A-infected mice received a daily intraperitoneal injection of 25mg/kg of GDC-0449, a Hh inhibitor, or vehicle, DMSO. As the control groups, mice without *Pb*A infection were injected with equal volume or concentration of vehicle or GDC-0449. Any significant changes were not detected in the control groups, indicating that DMSO and GDC-0449 rarely impacted on livers of control groups (Fig. 6). However, morphological injury and the increased ratio of liver weight to body weight (LW/BW) and serum ALT/AST levels were observed in the *Pb*A infected group with vehicle (10%+DMSO), whereas these morphological and physiological damages were significantly alleviated in the *Pb*A infected group with Hh inhibitor (10%+GDC-0449) (Fig. 6A and B). Increased expression of SMO and GLI2 in the 10%+DMSO group was down-regulated in 10%+GDC-0449 group (Fig. 6C and 6D). Upregulated pro-inflammatory markers, *Tnfa*, *Il1b* and *Cxcl1*, and in 10%+DMSO group were significantly down-regulated in 10%+GDC-0449 group, as assessed by qRT-PCR (Fig. 7A). In

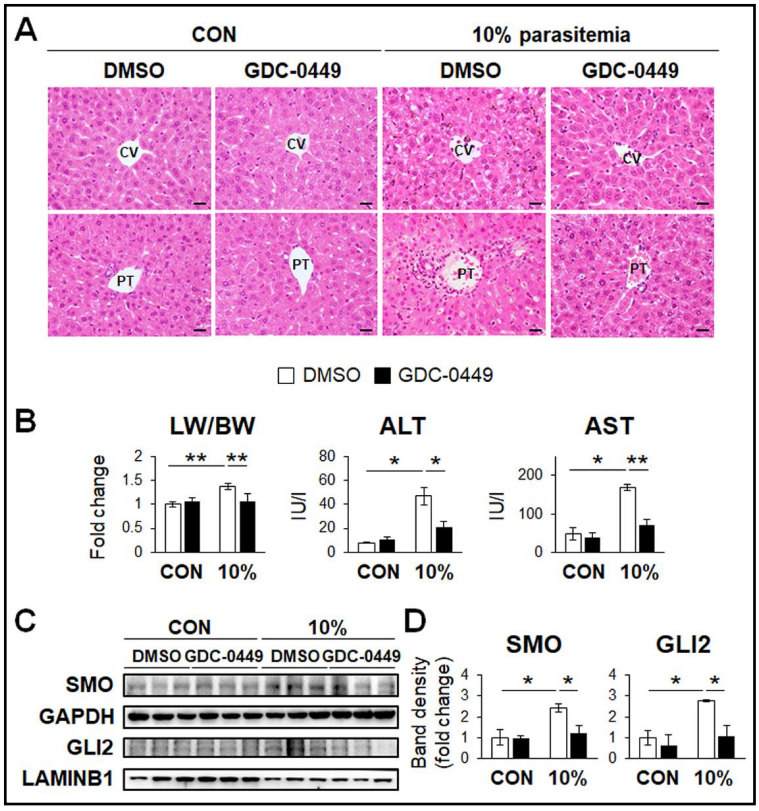

Fig. 6. Hh inhibition ameliorates liver injury in the malaria-infected liver. (A) Representative images of H&E-stained liver sections from representative mice of each group (scale bar = 20 μm). (B) Relative liver weight (LW) to body weight (BW) and levels of AST/ALT in serum are graphed as Mean±SD (*p<0.05, **p<0.005). (C) Immunoblots for SMO and GLI2 in livers from each group (n≥ 3 mice / group). GAPDH or LAMINβ1 was used as an internal control. Data shown represent one of three experiments with similar results. (D) Cumulative densitometric analyses of SMO and GLI2 immunoblots are displayed as the mean±SD (*p<0.05, **p<0.005). (CON: uninfected controls; 10%: infected mice with 10% parasitemia).

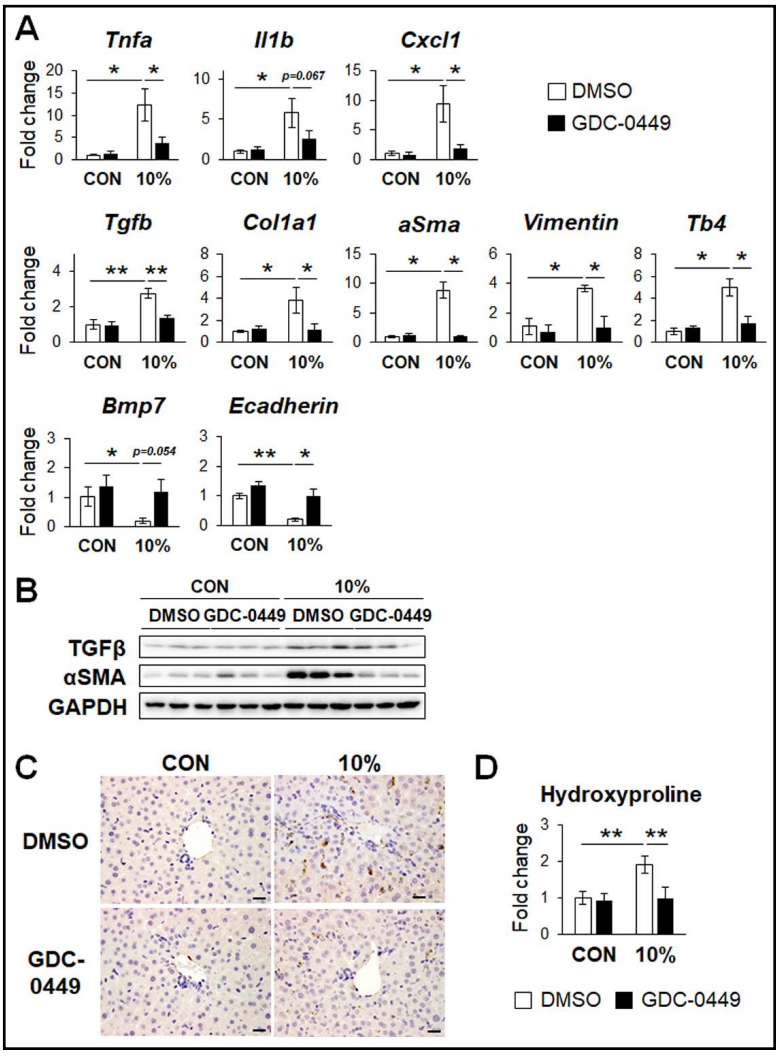

Fig. 7. Suppression of Hh reduces both inflammation and fibrosis in the malaria-infected liver. (A) QRT-PCR analysis for Tnfa, Il1b and Cxcl1, Tgfb, Col1a1, aSma, Vimentin, Tb4, Bmp7 and Ecadherin (n ≥ 3 mice / group). Mean±SD results are graphed (*p<0.05, **p<0.005). (B) Immunoblots and cumulative densitometric analyses for TGFβ and αSMA in livers from each group (n=3 mice / group). GAPDH was used as an internal control. Data shown represent one of three experiments with similar results. Results are displayed as the mean±SD (*p<0.05, **p<0.005). (C) Immunohistochemical staining for αSMA in liver sections from representative mice from each group. Brown colors indicate αSMA-positive cells (scale bar = 20 μm). (D) Hepatic hydroxyproline contents in liver tissues from each group (n = 3 mice / group). Mean±SD results are graphed (*p<0.05, **p<0.005). (CON: uninfected controls; 10%: infected mice with 10% parasitemia).

addition, increased levels of pro-fibrogenic markers, *Tgfb*, *Col1a1*, *aSma*, *Vimentin* and *Tb4*, and decreased levels of Q-HSC markers, *Bmp7* and *Ecadherin*, were reversed in 10%+GDC-0449 group. In line with mRNA expression, enhanced protein levels of TGFβ and αSMA in 10%+DMSO group declined in 10%+GDC-0449 group (Fig. 7B). Immunohistochemistry for αSMA showed the reduced accumulation of αSMA-positive cells in livers of the 10%+GDC-0449 compared with the 10%+DMSO group (Fig. 7C). Hydroxyproline contents also confirmed that the deposition of collagen fibrils was significantly lower in 10%+GDC-0449 the 10%+DMSO group (Fig. 7D). Taken together, these results demonstrated that the Hh suppression ameliorated liver damage and fibrosis in the *Pb*A-infected livers, suggesting that Hh signaling directly influenced liver response to *Pb*A infection.

Discussion

A wide range of hepatic dysfunction from mild to fulminant has been shown in patients infected with *P. falciparum* or *P. vivax* malaria, and a degree of liver damage has been reported to be related with the patient's medical history and characteristics, such as sex, age, and residence [1, 4, 8, 9, 35]. Such findings, however, have been mainly obtained from clinical

observations and patient-derived histopathology. A precise mechanism for explaining the development and progression of hepatic damage caused by malaria infection has been poorly investigated. Herein, we investigate the liver response to malaria infection using a murine model of blood-stage malaria infection. Although there is a limitation that injection of iRBCs into mice do not generate the liver stage of malaria parasites, many studies have reported that this murine model mimics clinical symptoms observed in human malaria [21-24, 36, 37]. It is possible that the blood stage of the malaria parasite is responsible for most clinical symptoms of malaria. In the present research, our experimental malaria model successfully replicated the pathophysiology of human malaria, including portal inflammation, hemozoin deposition, congestion, and steatosis in the infected liver (Fig. 1). In addition, we observed an accumulation of activated HSCs in the liver of our experimental model. Hence, this murine model could be a potential resource for investigating the pathological mechanisms of liver damage caused by malaria infection.

Infected erythrocytes are known to cytoadhere to small capillaries and post-capillary venules in host tissue, and this process is called sequestration [38, 39]. Liver is one of organs in which iRBCs preferentially accumulate to avoid immune system surveillance inside the spleen, and iRBC sequestration within the liver endothelium is now emerging as another factor that promotes liver damage [40-42]. Several studies suggest that iRBC sequestration contributes to the intrahepatic obstruction of blood flow, which leads to hepatocellular hypoxia and excessive intravascular hemolysis, causing increased oxidative stress and leukocyte infiltration [40, 43-45]. Infiltrated leukocytes also produce inflammatory mediators, thereby enhancing hepatic inflammation [43, 46]. In line with these findings, our study demonstrated that *Pb*A-iRBCs create a hypoxic environment in the liver, as demonstrated by HIF1 upregulation (Fig. 1F). Under hypoxic conditions, hepatocytes undergo apoptosis, whereas HSCs are activated and proliferate [47-50]. These apoptotic hepatocytes release various cytokines to stimulate HSCs and inflammation [16, 17]. Hh ligands released by apoptotic hepatocytes stimulate Hh-responsive cells, such as HSCs and liver progenitor cells [18, 19]. Given that Shh was upregulated in malaria-infected liver (Fig. 4), it is possible that apoptotic hepatocytes under hypoxic conditions release Shh, which triggers HSC activation, leading to liver fibrosis. The decreased HSC activation and fibrosis in Hh-inhibited liver infected with PbA also support this explanation (Figs 6 and 7). Hyperplasia of Kupffer cell that is commonly observed in injured liver is one of the most distinctive features of patients with malaria. It is caused by erythrophagocytosis with hemozoin which is a metabolic waste generated by parasites [9, 35, 51]. The highest amount of hemozoin is detected in liver (in comparison with other organs, including the spleen), and total hemozoin level parallels disease severity in murine malaria models [51-54]. Hemozoin activates macrophages by stimulating inflammatory signaling pathways, including Toll-like receptor 4 activation and NF-kB signaling. The activated macrophages produce inflammatory cytokines, such as IL-1b and TNF-a, which accelerate HSC activation, contributing to liver fibrosis [32, 46, 55-58]. In the present study, we found that Kupffer cell activation, hemozoin accumulation, and upregulation of pro-inflammatory genes were apparent in malaria-infected livers (Fig. 1). In line with our findings, it has been reported that inflammatory macrophages containing hemozoin in livers of malaria patients are involved in inducing liver fibrosis [35, 59, 60]. Therefore, these complicated liver responses against *Pb*A infection, including iRBC sequestration, hypoxia, increased apoptotic hepatocytes, and activation of HSC and Kupffer cells, may aggravate liver injury and fibrosis during blood stage malaria.

HSC activation is a common response to liver damage [12]. Inflammation also occurs in response to liver damage and it accelerates liver fibrosis by promoting the transition of Q-HSCs into MF-HSCs. In the present study, we examined the liver's response to *Pb*A infection with two different infection rates—10% and 30%—which resulted in enhanced inflammation and fibrosis in the *Pb*A-infected liver, demonstrating the upregulation of proinflammatory genes including *Tnfa*, *Il1b*, and *Cxcl1* (Fig. 1), and profibrotic genes including *Tgfb*, *Col1a1*, *aSma*, *Vimentin*, and *Tb4* (Figs 2 and 3). In addition, immunohistochemistry showed that the activated HSC-expressing αSMA accumulated in the livers of both infected

groups. Higher collagen content in the infected groups as assessed by hydroxyproline assay also supported the increased fibrosis in the livers of *Pb*A-infected mice. A growing body of evidence demonstrates that the Hh signaling pathway plays an important role in HSC transdifferentiation [13-15]. Increased expression of the Hh signaling pathway in these injured livers suggests that Hh signaling influenced the liver's responses to *Pb*A infection. Similarly, YAP has been reported to act as a critical regulator of HSC activation. Mannaerts et al. reported that YAP was activated and translocated into the nucleus during HSC activation [33]. These authors also showed that interference with YAP signaling reduced both HSC activation and fibrogenesis in the liver, suggesting that YAP is an essential regulator of HSC activation. In line with these findings, we report that net YAP activity was elevated in the fibrotic livers of mice at a *Pb*A infection rate of 30%. Although the level of Hh expression did not parallel the parasitemia infection rate (Fig. 4), the ratio of nuclear YAP/cytosolic YAP increased parallel to the level of parasitemia (Fig. 5). Hh expression and YAP signaling seem to be related in the liver's response, particularly HSC activation, to malaria-induced liver injury. Swiderska-Syn et al. recently demonstrated that the Hh pathway controls YAP activation in partial hepatectomized livers during liver regeneration [61]. They showed that blocking Hh signaling in HSCs inhibited activation of YAP, and deletion of YAP in HSCs suppressed Hh signaling, suggesting that Hh and YAP interact to maintain the MF-phenotype in HSCs. In addition, both Hh and YAP signaling were shown to be associated with TGFb in HSC activation and liver carcinogenesis [16, 62-64]. Compared with the 10% infection groups, a greater increase of TGFβ and αSMA protein in the 30% infection groups appears to have been promoted by enhanced YAP activity, suggesting the possibility that YAP accelerates HSC activation. Further studies are required to reveal the association of the Hh pathway with YAP in HSC transdifferentiation of the malaria-infected liver.

Conclusion

We demonstrated that HSCs are activated, and that Hh and YAP signaling are associated with this process, contributing to increased hepatic fibrosis in malaria-infected livers.

Abbreviations

α-SMA (α-smooth muscle actin); ALT (alanine aminotransferase); AST (aspartate aminotransferase); Col1α1 (collagen type 1 α 1); CXCL1 (chemokine (C-X-C motif) ligand 1); DAB (3, 3'-diaminobenzidine); DAPI (4',6-diamidino-2-phenylindole); DMSO (dimethyl sulfoxide); ECM (extracellular matrix); Gli (Gli-krüppel family member); Hh (Hedgehog); HIF (hypoxia inducible factor); HSC (hepatic stellate cell); IL (interleukin); MF-HSC (myofibroblastic hepatic stellate cells); *Pb*A (Plasmodium berghei ANKA); Shh (sonic hedgehog); Smo (smoothened); TGFβ (transforming growth factor-β); TNFα (tumor necrosis factor-α); YAP (yes-associated protein).

Acknowledgements

All authors declare no competing financial interests. This work was supported by 2-year grant of Pusan National University.

Disclosure Statement

All authors affirm that they have no conflicts of interest regarding this work.

References

1 Snow RW, Guerra CA, Noor AM, Myint HY, Hay SI: The global distribution of clinical episodes of Plasmodium falciparum malaria. Nature 2005;434:214-217.
2 Prudencio M, Mota MM, Mendes AM: A toolbox to study liver stage malaria. Trends Parasitol 2011;27:565-574.
3 Sturm A, Amino R, van de Sand C, Regen T, Retzlaff S, Rennenberg A, Krueger A, Pollok JM, Menard R, Heussler VT: Manipulation of host hepatocytes by the malaria parasite for delivery into liver sinusoids. Science 2006;313:1287-1290.
4 Mackintosh CL, Beeson JG, Marsh K: Clinical features and pathogenesis of severe malaria. Trends Parasitol 2004;20:597-603.
5 Adachi K, Tsutsui H, Kashiwamura S, Seki E, Nakano H, Takeuchi O, Takeda K, Okumura K, Van Kaer L, Okamura H, Akira S, Nakanishi K: Plasmodium berghei infection in mice induces liver injury by an IL-12- and toll-like receptor/myeloid differentiation factor 88-dependent mechanism. J Immunol 2001;167:5928-5934.
6 Adachi K, Tsutsui H, Seki E, Nakano H, Takeda K, Okumura K, Van Kaer L, Nakanishi K: Contribution of CD1d-unrestricted hepatic DX5+ NKT cells to liver injury in Plasmodium berghei-parasitized erythrocyte-injected mice. Int Immunol 2004;16:787-798.
7 Prommano O, Chaisri U, Turner GD, Wilairatana P, Ferguson DJ, Viriyavejakul P, White NJ, Pongponratn E: A quantitative ultrastructural study of the liver and the spleen in fatal falciparum malaria. Southeast Asian J Trop Med Public Health 2005;36:1359-1370.
8 Sowunmi A: Hepatomegaly in acute falciparum malaria in children. Trans R Soc Trop Med Hyg 1996;90:540-542.
9 Shah S, Ali L, Sattar RA, Aziz T, Ansari T, Ara J: Malarial hepatopathy in falciparum malaria. J Coll Physicians Surg Pak 2009;19:367-370.
10 Bhalla A, Suri V, Singh V: Malarial hepatopathy. J Postgrad Med 2006;52:315-320.
11 Jain A, Kaushik R, Kaushik RM: Malarial hepatopathy: Clinical profile and association with other malarial complications. Acta Trop 2016;159:95-105.
12 Bataller R, Brenner DA: Liver fibrosis. J Clin Invest 2005;115:209-218.
13 Sicklick JK, Li YX, Choi SS, Qi Y, Chen W, Bustamante M, Huang J, Zdanowicz M, Camp T, Torbenson MS, Rojkind M, Diehl AM: Role for hedgehog signaling in hepatic stellate cell activation and viability. Lab Invest 2005;85:1368-1380.
14 Choi SS, Omenetti A, Witek RP, Moylan CA, Syn WK, Jung Y, Yang L, Sudan DL, Sicklick JK, Michelotti GA, Rojkind M, Diehl AM: Hedgehog pathway activation and epithelial-to-mesenchymal transitions during myofibroblastic transformation of rat hepatic cells in culture and cirrhosis. Am J Physiol Gastrointest Liver Physiol 2009;297:G1093-1106.
15 Yang L, Wang Y, Mao H, Fleig S, Omenetti A, Brown KD, Sicklick JK, Li YX, Diehl AM: Sonic hedgehog is an autocrine viability factor for myofibroblastic hepatic stellate cells. J Hepatol 2008;48:98-106.
16 Omenetti A, Choi S, Michelotti G, Diehl AM: Hedgehog signaling in the liver. J Hepatol 2011;54:366-373.
17 Machado MV, Diehl AM: Hedgehog Signaling in Liver Pathophysiology. J Hepatol 2018;68:550-562.
18 Jung Y, Witek RP, Syn WK, Choi SS, Omenetti A, Premont R, Guy CD, Diehl AM: Signals from dying hepatocytes trigger growth of liver progenitors. Gut 2010;59:655-665.
19 Rangwala F, Guy CD, Lu J, Suzuki A, Burchette JL, Abdelmalek MF, Chen W, Diehl AM: Increased production of sonic hedgehog by ballooned hepatocytes. J Pathol 2011;224:401-410.
20 Guha M, Kumar S, Choubey V, Maity P, Bandyopadhyay U: Apoptosis in liver during malaria: role of oxidative stress and implication of mitochondrial pathway. Faseb J 2006;20:1224-1226.
21 Griffith JW, O'Connor C, Bernard K, Town T, Goldstein DR, Bucala R: Toll-like receptor modulation of murine cerebral malaria is dependent on the genetic background of the host. J Infect Dis 2007;196:1553-1564.
22 Yanez DM, Manning DD, Cooley AJ, Weidanz WP, van der Heyde HC: Participation of lymphocyte subpopulations in the pathogenesis of experimental murine cerebral malaria. J Immunol 1996;157:1620-1624.
23 de Kossodo S, Grau GE: Profiles of cytokine production in relation with susceptibility to cerebral malaria. J Immunol 1993;151:4811-4820.

24 Baptista FG, Pamplona A, Pena AC, Mota MM, Pied S, Vigario AM: Accumulation of Plasmodium berghei-infected red blood cells in the brain is crucial for the development of cerebral malaria in mice. Infect Immun 2010;78:4033-4039.
25 Grau GE, Piguet PF, Engers HD, Louis JA, Vassalli P, Lambert PH: L3T4+ T lymphocytes play a major role in the pathogenesis of murine cerebral malaria. J Immunol 1986;137:2348-2354.
26 Wang S, Lee Y, Kim J, Hyun J, Lee K, Kim Y, Jung Y: Potential role of Hedgehog pathway in liver response to radiation. PLoS One 2013;8:e74141.
27 Oancea I, Png CW, Das I, Lourie R, Winkler IG, Eri R, Subramaniam N, Jinnah HA, McWhinney BC, Levesque JP, McGuckin MA, Duley JA, Florin TH: A novel mouse model of veno-occlusive disease provides strategies to prevent thioguanine-induced hepatic toxicity. Gut 2013;62:594-605.
28 Kim J, Wang S, Hyun J, Guy CD, Jung Y: Hedgehog Signaling is Associated with Liver Response to Fractionated Irradiation in Mice. Cell Physiol Biochem 2016;40:263-276.
29 Hioki A, Yoshino M, Kano S, Ohtomo H: Pathophysiology of hypoxia in mice infected with Plasmodium berghei. Parasitol Res 1987;73:298-302.
30 Koyama Y, Brenner DA: Liver inflammation and fibrosis. J Clin Invest 2017;127:55-64.
31 Pradere JP, Kluwe J, De Minicis S, Jiao JJ, Gwak GY, Dapito DH, Jang MK, Guenther ND, Mederacke I, Friedman R, Dragomir AC, Aloman C, Schwabe RF: Hepatic macrophages but not dendritic cells contribute to liver fibrosis by promoting the survival of activated hepatic stellate cells in mice. Hepatology 2013;58:1461-1473.
32 Wynn TA, Barron L: Macrophages: master regulators of inflammation and fibrosis. Semin Liver Dis 2010;30:245-257.
33 Mannaerts I, Leite SB, Verhulst S, Claerhout S, Eysackers N, Thoen LF, Hoorens A, Reynaert H, Halder G, van Grunsven LA: The Hippo pathway effector YAP controls mouse hepatic stellate cell activation. J Hepatol 2015;63:679-688.
34 Zhao B, Li L, Tumaneng K, Wang CY, Guan KL: A coordinated phosphorylation by Lats and CK1 regulates YAP stability through SCF(beta-TRCP). Genes Dev 2010;24:72-85.
35 Viriyavejakul P, Khachonsaksumet V, Punsawad C: Liver changes in severe Plasmodium falciparum malaria: histopathology, apoptosis and nuclear factor kappa B expression. Malar J 2014;13:106.
36 Taniguchi T, Miyauchi E, Nakamura S, Hirai M, Suzue K, Imai T, Nomura T, Handa T, Okada H, Shimokawa C, Onishi R, Olia A, Hirata J, Tomita H, Ohno H, Horii T, Hisaeda H: Plasmodium berghei ANKA causes intestinal malaria associated with dysbiosis. Sci Rep 2015;5:15699.
37 Craig AG, Grau GE, Janse C, Kazura JW, Milner D, Barnwell JW, Turner G, Langhorne J: The role of animal models for research on severe malaria. PLoS Pathog 2012;8:e1002401.
38 El-Assaad F, Wheway J, Mitchell AJ, Lou J, Hunt NH, Combes V, Grau GE: Cytoadherence of Plasmodium berghei-infected red blood cells to murine brain and lung microvascular endothelial cells *in vitro*. Infect Immun 2013;81:3984-3991.
39 Pongponratn E, Riganti M, Punpoowong B, Aikawa M: Microvascular sequestration of parasitized erythrocytes in human falciparum malaria: a pathological study. Am J Trop Med Hyg 1991;44:168-175.
40 Medeiros MM, da Silva HB, Reis AS, Barboza R, Thompson J, Lima MR, Marinho CR, Tadokoro CE: Liver accumulation of Plasmodium chabaudi-infected red blood cells and modulation of regulatory T cell and dendritic cell responses. PLoS One 2013;8:e81409.
41 Langreth SG, Peterson E: Pathogenicity, stability, and immunogenicity of a knobless clone of Plasmodium falciparum in Colombian owl monkeys. Infect Immun 1985;47:760-766.
42 Fonager J, Pasini EM, Braks JA, Klop O, Ramesar J, Remarque EJ, Vroegrijk IO, van Duinen SG, Thomas AW, Khan SM, Mann M, Kocken CH, Janse CJ, Franke-Fayard BM: Reduced CD36-dependent tissue sequestration of Plasmodium-infected erythrocytes is detrimental to malaria parasite growth *in vivo*. J Exp Med 2012;209:93-107.
43 Dey S, Bindu S, Goyal M, Pal C, Alam A, Iqbal MS, Kumar R, Sarkar S, Bandyopadhyay U: Impact of intravascular hemolysis in malaria on liver dysfunction: involvement of hepatic free heme overload, NF-kappaB activation, and neutrophil infiltration. J Biol Chem 2012;287:26630-26646.
44 Brugat T, Cunningham D, Sodenkamp J, Coomes S, Wilson M, Spence PJ, Jarra W, Thompson J, Scudamore C, Langhorne J: Sequestration and histopathology in Plasmodium chabaudi malaria are influenced by the immune response in an organ-specific manner. Cell Microbiol 2014;16:687-700.

45 van der Heyde HC, Nolan J, Combes V, Gramaglia I, Grau GE: A unified hypothesis for the genesis of cerebral malaria: sequestration, inflammation and hemostasis leading to microcirculatory dysfunction. Trends Parasitol 2006;22:503-508.
46 Jaramillo M, Plante I, Ouellet N, Vandal K, Tessier PA, Olivier M: Hemozoin-inducible proinflammatory events *in vivo*: potential role in malaria infection. J Immunol 2004;172:3101-3110.
47 Moon JO, Welch TP, Gonzalez FJ, Copple BL: Reduced liver fibrosis in hypoxia-inducible factor-1alpha-deficient mice. Am J Physiol Gastrointest Liver Physiol 2009;296:G582-592.
48 Copple BL, Bustamante JJ, Welch TP, Kim ND, Moon JO: Hypoxia-inducible factor-dependent production of profibrotic mediators by hypoxic hepatocytes. Liver Int 2009;29:1010-1021.
49 Liu J, Li Y, Liu L, Wang Z, Shi C, Cheng Z, Zhang X, Ding F, Chen PS: Double Knockdown of PHD1 and Keap1 Attenuated Hypoxia-Induced Injuries in Hepatocytes. Front Physiol 2017;8:291.
50 Mesarwi OA, Shin MK, Bevans-Fonti S, Schlesinger C, Shaw J, Polotsky VY: Hepatocyte Hypoxia Inducible Factor-1 Mediates the Development of Liver Fibrosis in a Mouse Model of Nonalcoholic Fatty Liver Disease. PLoS One 2016;11:e0168572.
51 Whitten R, Milner DA, Jr., Yeh MM, Kamiza S, Molyneux ME, Taylor TE: Liver pathology in Malawian children with fatal encephalopathy. Hum Pathol 2011;42:1230-1239.
52 Anand AC, Puri P: Jaundice in malaria. J Gastroenterol Hepatol 2005;20:1322-1332.
53 Frita R, Carapau D, Mota MM, Hanscheid T: *In vivo* Hemozoin Kinetics after Clearance of Plasmodium berghei Infection in Mice. Malar Res Treat 2012;2012:373086.
54 Levesque MA, Sullivan AD, Meshnick SR: Splenic and hepatic hemozoin in mice after malaria parasite clearance. J Parasitol 1999;85:570-573.
55 Barrera V, Skorokhod OA, Baci D, Gremo G, Arese P, Schwarzer E: Host fibrinogen stably bound to hemozoin rapidly activates monocytes via TLR-4 and CD11b/CD18-integrin: a new paradigm of hemozoin action. Blood 2011;117:5674-5682.
56 Jaramillo M, Godbout M, Olivier M: Hemozoin induces macrophage chemokine expression through oxidative stress-dependent and -independent mechanisms. J Immunol 2005;174:475-484.
57 Jaramillo M, Gowda DC, Radzioch D, Olivier M: Hemozoin increases IFN-gamma-inducible macrophage nitric oxide generation through extracellular signal-regulated kinase- and NF-kappa B-dependent pathways. J Immunol 2003;171:4243-4253.
58 Preisser L, Miot C, Le Guillou-Guillemette H, Beaumont E, Foucher ED, Garo E, Blanchard S, Fremaux I, Croue A, Fouchard I, Lunel-Fabiani F, Boursier J, Roingeard P, Cales P, Delneste Y, Jeannin P: IL-34 and macrophage colony-stimulating factor are overexpressed in hepatitis C virus fibrosis and induce profibrotic macrophages that promote collagen synthesis by hepatic stellate cells. Hepatology 2014;60:1879-1890.
59 Rupani AB, Amarapurkar AD: Hepatic changes in fatal malaria: an emerging problem. Ann Trop Med Parasitol 2009;103:119-127.
60 Mimche PN, Brady LM, Bray CF, Lee CM, Thapa M, King TP, Quicke K, McDermott CD, Mimche SM, Grakoui A, Morgan ET, Lamb TJ: The receptor tyrosine kinase EphB2 promotes hepatic fibrosis in mice. Hepatology 2015;62:900-914.
61 Swiderska-Syn M, Xie G, Michelotti GA, Jewell ML, Premont RT, Syn WK, Diehl AM: Hedgehog regulates yes-associated protein 1 in regenerating mouse liver. Hepatology 2016;64:232-244.
62 Zhang K, Chang Y, Shi Z, Han X, Han Y, Yao Q, Hu Z, Cui H, Zheng L, Han T, Hong W: omega-3 PUFAs ameliorate liver fibrosis and inhibit hepatic stellate cells proliferation and activation by promoting YAP/TAZ degradation. Sci Rep 2016;6:30029.
63 Javelaud D, Pierrat MJ, Mauviel A: Crosstalk between TGF-beta and hedgehog signaling in cancer. FEBS Lett 2012;586:2016-2025.
64 Nishio M, Sugimachi K, Goto H, Wang J, Morikawa T, Miyachi Y, Takano Y, Hikasa H, Itoh T, Suzuki SO, Kurihara H, Aishima S, Leask A, Sasaki T, Nakano T, Nishina H, Nishikawa Y, Sekido Y, Nakao K, Shin-Ya K et al.: Dysregulated YAP1/TAZ and TGF-beta signaling mediate hepatocarcinogenesis in Mob1a/1b-deficient mice. Proc Natl Acad Sci U S A 2016;113:E71-80.